

Laser-combined Scanning Tunneling Microscopy and Its Applications

HIDEMI SHIGEKAWA, AND SHOJI YOSHIDA
FACULTY OF PURE AND APPLIED SCIENCES, UNIVERSITY OF TSUKUBA

ABSTRACT

With size reduction, the differences in the electronic properties of materials and current devices, for example, caused by the structural nonuniformity in each element, have an ever more crucial effect on macroscopic functions. For further advances of nanoscale science and technology, development of a method for exploring transient dynamics of local quantum functions in organized small structures is essential. Here, we review laser-combined scanning tunneling microscopy (STM) which enables real space imaging of nanoscale quantum dynamics even in the femtosecond range.

INTRODUCTION

The understanding and control of quantum dynamics, such as transition and transport in nanoscale structures, are the key factors for continuing the advance of nanoscale science and technology. However, with size reduction, the differences in the electronic properties of materials and current devices, for example, caused by the structural nonuniformity in each element, have an ever more crucial effect on the macroscopic functions. That is, atomic-scale defects, for example, have markedly changed the entire situation: defects, which were once considered as a problem to be avoided, are actively designed and controlled to realize desired functions. The fluctuation in the distribution of dopant materials governs the characteristic properties of macroscopic functions. Therefore, for further advances in nanoscale science and technology, development of a method for exploring transient dynamics of local quantum functions in organized small structures is essential.

Since the development of scanning tunneling microscopy (STM), the direct imaging of atomic-scale structures has been lifting the veil from various longstanding problems and extending the frontiers of science and technology [1-3]. In STM, a sharp tip is placed above the target material, and we obtain information just below the probe tip through the measurement of tunnel current, spin, force and so on (Fig. 1). In a basic STM, the bias voltage applied between the tip and the sample is adjusted and the corresponding change in tunneling current is measured. To obtain further information, additional parameters, such as temperature, magnetic field, and tip-sample distance, are modulated depending on the purpose. An attractive option is to combine optical technologies with scanning probe microscopy (SPM), and many efforts have been devoted to developing various techniques

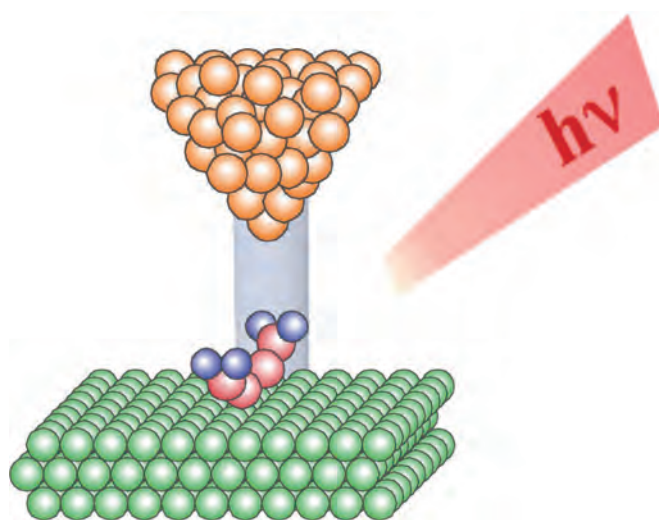


Fig. 1: Schematic illustration imaging SPM combined with optical technologies.

[4-6]. For example, near-field scanning optical microscopy (NSOM) is used not only for spectroscopy but also for manufacturing nanoscale structures [7-9], and STM combined with synchrotron radiation has been opening the door to characterizing atomic species by exciting core level electrons [10-13]. In this paper, we review laser-combined STM based on what we have been developing.

STM combined with a continuous-wave laser

In this section, several techniques realized by combining a continuous-wave (CW) laser with STM are overviewed.

Direct observation of single molecule photoisomerization

Photoisomerization plays important roles in realizing various attractive functions and has been extensively studied [14-16]. Here, laser-combined STM was applied to directly observe the structural change of azobenzene, a typical molecule with the characteristic of photoisomerization, which shows trans- or cis-conformation under visible or ultraviolet photoillumination, respectively (Fig. 2(a)) [17]. Isolated azomolecules were prepared in a self-assembled monolayer (SAM) on a Au substrate with dodecanethiol molecules as a spacer, and a photoinduced change was observed by STM. By alternately changing the wavelength of a He-Cd laser between a visible (440 nm) and an ultraviolet (360 nm), the photoinduced structural change of a single molecule between trans- and cis-conformations was directly imaged, as shown in Fig. 2(b). Using STM, the electronic structures associated with the structural change can be investigated. Rectification behavior in current-bias voltage (I / V) characteristics, which was predicted by Ratner et al. [18], was produced by the switching of the two conformations.

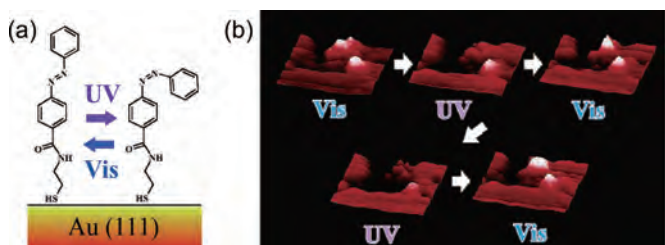


Fig. 2: (a) Photoisomerization of azobenzene, (b) STM images of photoisomerization of single azobenzene molecule.

Optical doping for controlling phase transition

Charge transfer is one of the key factors for governing the mechanisms in various physical systems. In-wire/Si is a typical structure with a characteristic metal-insulator phase transition [19, 20]. However, the critical tempera-

tures obtained by several groups showed large variations [21]. By analyzing the STM image of the phase transition depending on the laser intensity and bias voltage, it was shown that inhomogeneous charge transfer exists at the metal/semiconductor interface, depending on the distribution of the atomic-scale defects in each area (Fig. 3) [22]. The spatial variation in the band filling at the interface depending on the sample condition results in the observed variation in critical temperature. On the basis of this mechanism, the phase transition was actively controlled by changing the amount of charge transfer using the combination of the bias voltage applied between the tip and the sample and the intensity of photoillumination. Namely, the balance between the tip-induced band bending (TIBB) and the laser intensity determines surface photovoltage (SPV) that induces a rapid change in

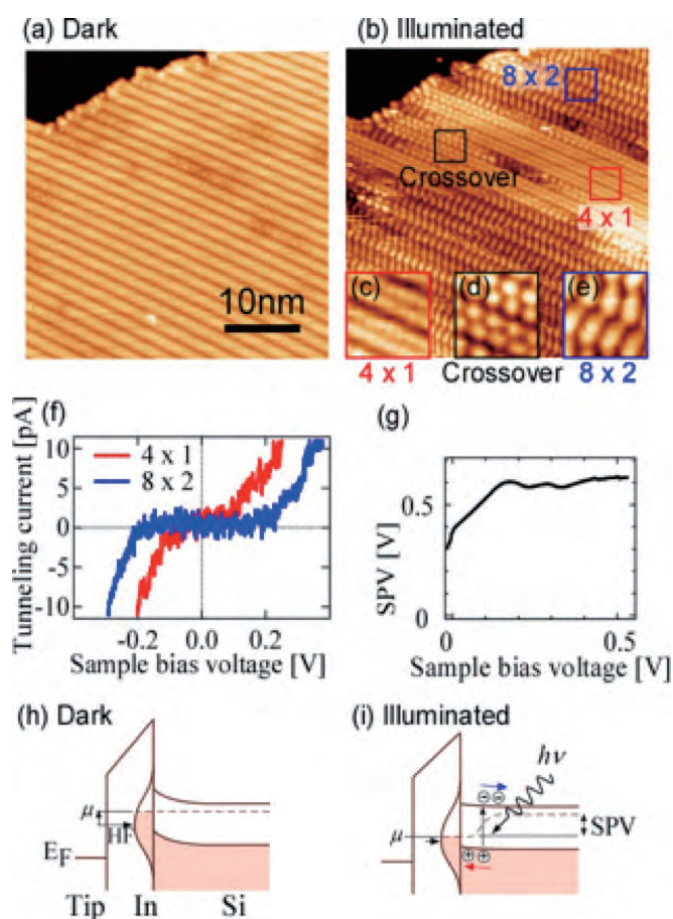


Fig. 3: STM images of In/Si surface obtained at 61 K (a) without and (b) with illumination. The metal phase ((c) and (f)) changes into the insulator phase ((e) and (f)) with photoillumination due to the change in band filling depending on the balance between TIBB (tip-induced band bending) and SPV (surface photovoltage) in each area ((g) to (i)). (d) Crossover phase. The balance was controlled by the combination of the bias voltage applied between the tip and the sample and the laser intensity.

the band filling of the local area. Rapid and local switching of conductance is considered to make the phase transition more applicable than the control by temperature.

Light-modulated STS (LT-STS) analysis on local potential

In STM on a semiconductor, a nanoscale metal-insulator-semiconductor (MIS) junction is formed by the STM tip, tunneling gap, and sample (Fig. 4). For a reverse bias voltage condition between the STM tip and sample, bias voltage leakage causes TIBB. With optical illumination, the redistribution of photocarriers reduces the electric field, thereby flattening the band bending, i.e., SPV. By comparing the *I-V* curves measured in the dark and in illuminated conditions, we can obtain information about the band bending under the dark condition. When carriers are injected, owing to a mechanism similar to SPV, the band bending is reduced. Therefore, by measuring the value of SPV over the surface, we can map the carrier distribution as well as the potential landscape in the corresponding area.

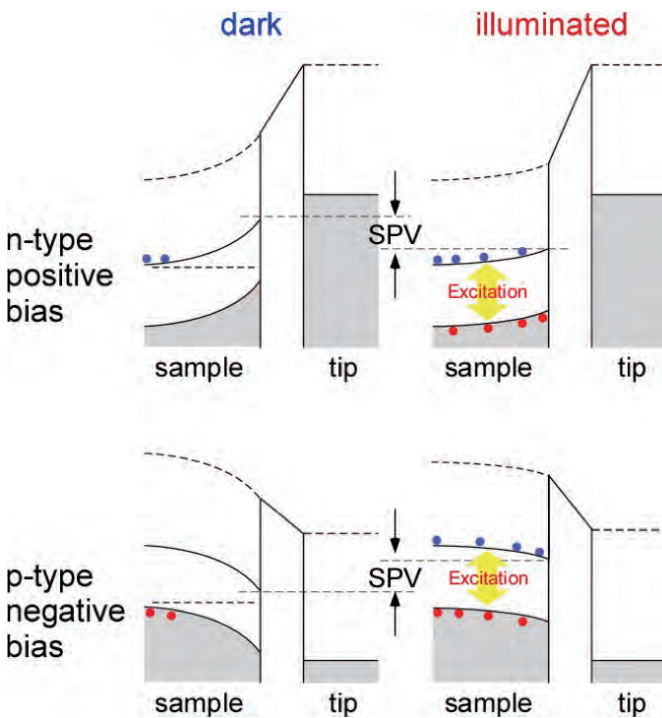


Fig. 4: Nanoscale metal-insulator-semiconductor (MIS) structure formed by the STM junction under reverse bias voltage conditions. TIBB under the dark condition is reduced by charge injection as well as SPV.

There are several ways to obtain the information on SPV [23-26]. One method we have developed is light-modulated STS (LM-STS), where the *I-V* curve is measured under chopped photoillumination (Fig. 5) [26, 27]. The *I-V*

curves under dark and photoilluminated conditions are obtained simultaneously, and from the amount of shift between the two *I-V* curves, SPV at a required bias voltage is determined.

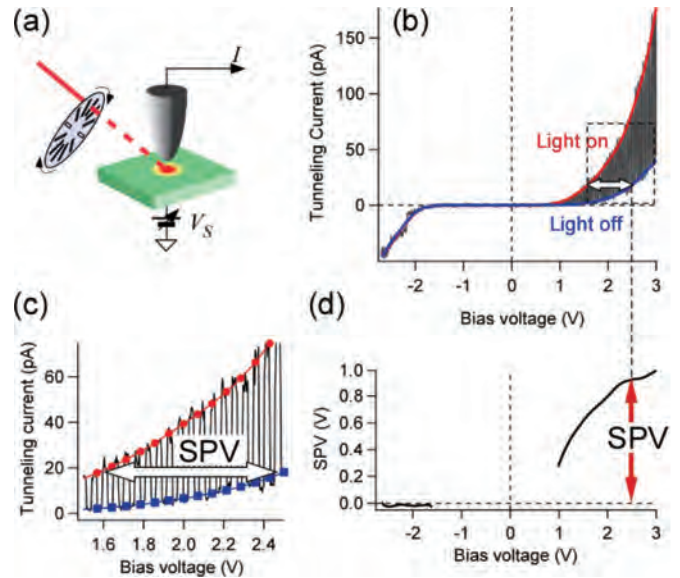


Fig. 5: (a) Schematic illustrations of light-modulated STS (LT-STS). (b) The *I-V* curve is measured under illumination with a chopped light (typically 1 kHz). Bias-voltage-dependent SPV is determined to be related to the bias voltage for the dark condition here from the shift of the two *I-V* curves ((c) and (d)).

Figure 6 shows an example of the imaging of the hole injection process in a GaAs p-n junction in real space [27]. Holes are injected by increasing the forward bias voltage

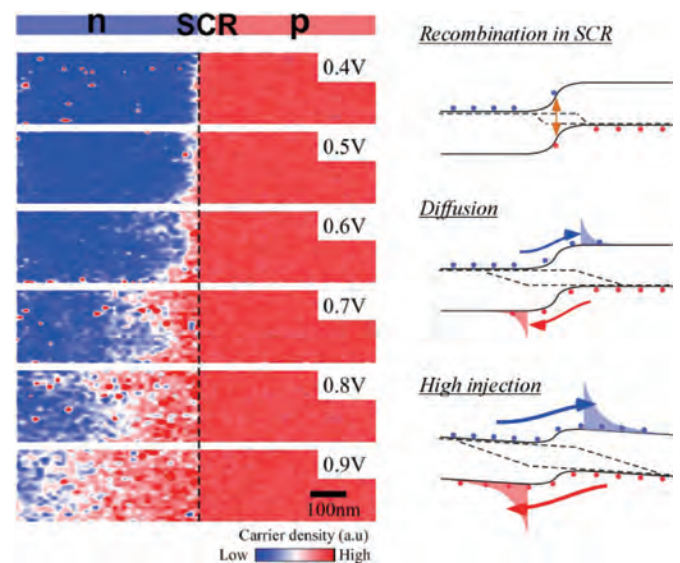


Fig. 6: Nanoscale mapping of hole injection in GaAs pn junction with increasing forward bias voltage (blue to red). Band structures corresponding to the conditions are shown on the right side. SCR: space charge region.

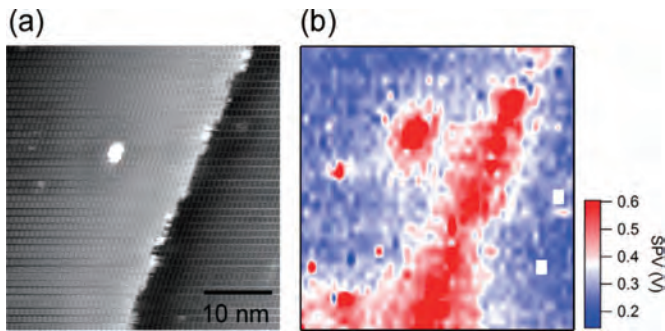


Fig. 7: STM image and potential mapping around atomic-scale defects on GaAs surface obtained by LM-STs.

applied to the p-n junction. Since a reverse bias voltage condition is necessary to observe SPV, only the left half of each image is considered here. To observe the carrier dynamics on the right side, we need to switch the sign of bias voltage. Instead of a uniform current flow, we can see a large fluctuation in current on the nanoscale. This may be attributed to an interface problem, but as shown in the images in Fig. 7 obtained by the same technique, local potential is modulated by atomic-scale defects [28], which affects the local carrier dynamics, and therefore, macroscopic functions. Furthermore, the size of the image in Fig. 7 is similar to the target size of current semiconductor devices, suggesting the importance of the

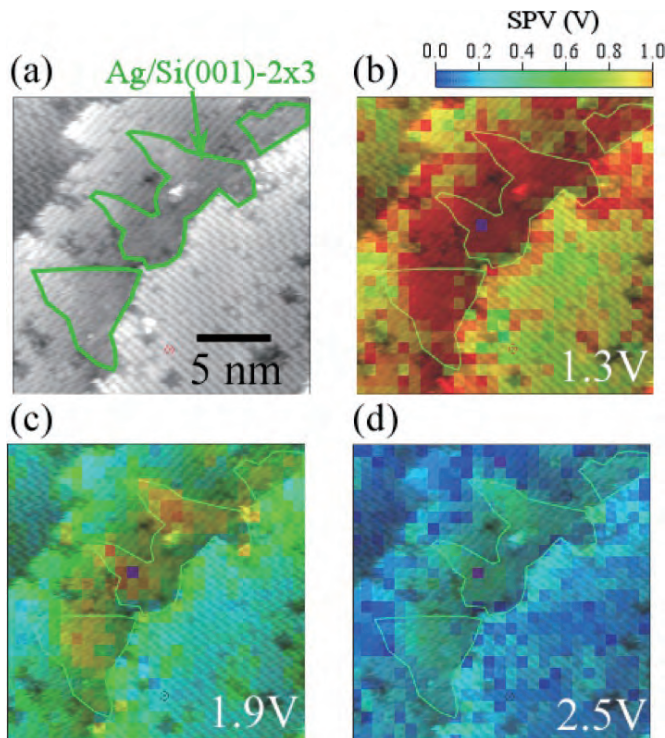


Fig. 8: Bias voltage dependence of SPV mapping obtained by LM-STs on Ag/Si(001) surface (30 nm × 30 nm).

time-resolved (TR) analysis of such carrier dynamics for further advances.

In addition to the 2D information, the question of how to analyze the depth profile of the electronic structures should be answered. Since SPV originates from TIBB related to the depletion layer of the sample surface induced by bias voltage leakage, one option is to control the area of the depletion layer by changing the bias voltage. Figure 8 shows the SPV mapping of Ag/Si depending on the bias voltage applied between the STM tip and sample. The spatial distribution of SPV clearly changes with the bias voltage, showing the possibility of three-dimensional (3D) analysis on semiconductors with nanostructures. This bias-voltage-dependent analysis is considered to be applicable to the TR-STM measurement discussed in 3.3.

STM combined with an ultrashort-pulse laser

In this section, ultrashort-pulse laser technology is combined with STM to obtain additional information on the local carrier dynamics in materials and devices.

Optical pump-probe (OPP) method

One of the most promising methods in laser-combined STM is the optical pump-probe method (Fig. 9) [29, 30]. When ultrashort laser pulses are produced, for example, at a typical repetition frequency of 80 MHz, the original pulse train has a time difference of about 13 ns between two subsequent pulses, as shown in Fig. 9(b) (upper train). Each pulse is divided into two pulses with a certain delay time to form a train of pulse pairs (lower train), which are called pump and probe pulses. The delay time can be controlled by changing the optical length of the delay line system (Fig. 9(c)). In general, the optical length is changed by the mechanical drive of reflecting mirrors along the delay line. How to use the pump and probe pulses depends on the purpose.

Atomic-scale manipulation

A simple way to observe the change in an STM image after photoexcitation is as follows. For example, we can excite selected phonon modes coherently, as well as the electronic transition [30, 31]. Here, the periodicity of ultrashort laser pulses was tuned to excite the phonon modes of Si-7 × 7 adatoms, which are site-dependent among 4 different states, i.e., faulted, unfaulted, corner and center adatoms [32, 33]. After each irradiation with a different repetition rate, the number of adatoms desorbed was counted. Similar to the manipulation by

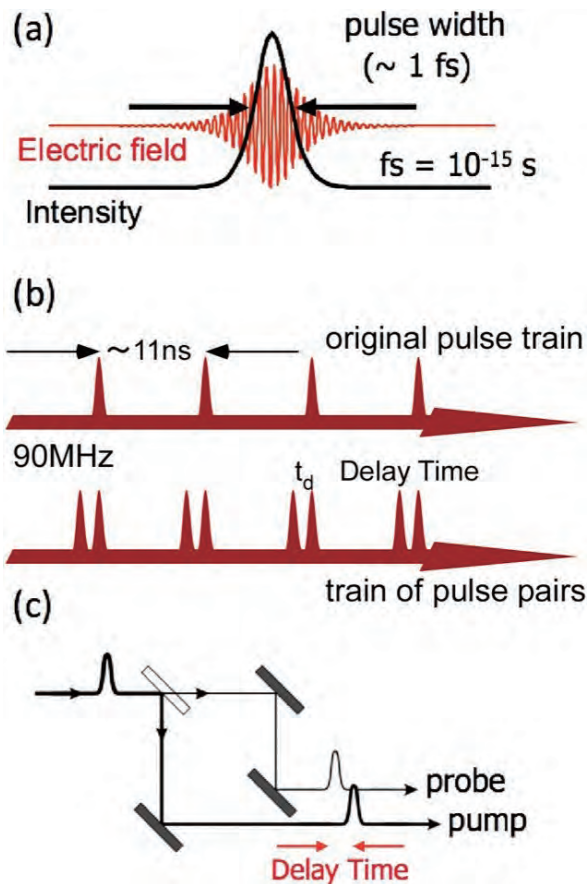


Fig. 9: Schematic illustrations of optical pump-probe (OPP) method: (a) ultrashort optical pulse, (b) original and modified pulse trains, and (c) delay line system.

the inelastic tunneling technique [34, 35], adatoms were selectively manipulated. With this technique, a large area can be simultaneously modulated. Control of phase transition by coherent phonon excitation is an attractive target of current research [36].

Time-resolved STM (TR-STM)

The spatial resolution of STM is excellent. We can see individual atoms and electronic structural properties such as the local density of states with atomic resolution. Since the development of STM, the direct imaging of atomic-scale structures has been lifting the veil from various longstanding problems and extending the frontiers of science and technology [1-3]. However, since the temporal resolution of STM is limited to less than 100 kHz owing to the circuit bandwidth [37-39], the ultrafast dynamics in materials has been beyond its field of vision. In contrast, the advances in ultrashort-pulse laser technology have opened the door to the world of ultrafast phenomena. A prominent method is OPP measure-

ment, which has enabled us to observe ultrafast dynamics in the femtosecond range. However, the spatial resolution of such optical methods is limited, in general, by the wavelength. Therefore, it has been one of the most challenging goals to combine STM with ultrashort-pulse laser technology since the development of STM in 1982 [1]. There is a long history on this issue, and many efforts were made in various ways [5, 40-45]. In this review, we focus on the laser-combined STM developed based on the OPP method.

OPP method for time-resolved measurement

To use the OPP method for time-resolved analysis, the first pulse is used as a pump to excite the sample surface and the second pulse is used as a probe to observe the relaxation of the excited states induced by the pump pulse. When carriers excited by the first pulse, for example, remain in the excited states, absorption of the second pulse is suppressed depending on the delay time, which is called absorption bleaching.

Therefore, if the reflectivity of the second pulse (probe pulse), for example, is measured as a function of delay time, we can obtain information on the relaxation of the excited state induced by the first pulse (pump pulse) through the change in the reflectivity of the probe pulse. In this case, the time resolution is limited only by the pulse width, i.e., in the femtosecond range.

In the new microscopy technique, the sample surface below the STM tip is excited by a paired-pulse train with a certain delay time t_d , that is similar to the OPP method, but the signal is the tunnel current I , instead of the change in the reflectivity of the probe pulse, as a function of delay time. The optical pulses give rise to current pulses in the raw tunneling current I^* , which reflects the excitation and relaxation of the sample. If these current pulses decay fast compared with the time scale of the STM preamplifier bandwidth, they are temporally averaged in the preamplifier and cannot be detected directly in the signal I . Even in such a case, the relaxation dynamics can be probed through the delay time dependence of I . By combining STM with ultrashort pulse laser technologies, the spatial resolution of STM and the temporal resolution of an ultrashort pulse laser in the femtosecond range are simultaneously achieved. Since signals are weak, we need to use the lock-in detection method. There, the excitation is oscillated at a certain frequency and the corresponding signal change is measured. In general, laser intensity is modulated in the OPP method,

which, however, causes thermal expansion of the STM tip and sample. Since a 0.1 nm change in tip-sample distance produces one order change in tunneling current, it is difficult to detect the weak signal under this condition. A promising option is to modulate the delay time between the pump and probe pulses instead of intensity. With this modulation technique, laser intensity is not changed and we can choose the modulation frequency independent of the noise frequency originating from thermal expansions [46].

TR-signal from a semiconductor

What type of signal can be observed? TIBB appears under a reverse bias voltage condition. With photoillumination, the redistribution of the photocarriers reduces the band bending, i.e., SPV. Then, the excited state subsequently relaxes to the original state through two processes. One is the decay of the photocarriers on the bulk side via recombination, drift and diffusion. We call this bulk-side decay. The other is the decay of the minority carriers trapped at the surface via recombination and thermionic emission, which we call surface-side decay.

When the second pulse arrives during the bulk-side decay, the carrier density induced by the second pulse decreases

due to absorption bleaching. In such a case, the amount of surface photovoltage, thus, the total tunneling current, changes depending on the delay time. On the other hand, when the second pulse arrives during the surface-side decay, the photocarriers are less trapped at the surface owing to the existence of SPV induced by the first pulse, resulting in change in the total tunneling current depending on the delay time. Therefore, by measuring the tunneling current as a function of delay time, we can obtain information about the carrier dynamics in both processes.

Figure 10 shows time-resolved spectra of the bulk-side decay obtained for various samples [46]. With the new method, carrier dynamics can be measured over a wide range of time scales using one microscope. Therefore, we can evaluate the carrier dynamics in organized small structures consisting of composite materials with pinpoint accuracy. Furthermore, as has been shown, although the new microscopy technique is based on the optical pump-probe method, since the probe is a tunneling current, we can obtain local information at the nano-scale level, which cannot be measured by a conventional OPP method, such as diffusion, drift and the effects of atomic-scale defects on the carrier dynamics.

Applications of time-resolved STM

In this section, two examples of the OPP-STM measurement are shown.

Nanoparticle/semiconductor interface

The understanding and control of quantum dynamics in nanoparticles and their interfaces with surrounding materials are important and play essential roles in various fields, such as semiconductor devices, catalyst actions, and energy transfer. Here, as an example, OPP-STM is carried out on a metal-nanoparticle/semiconductor structure [46].

When Co is deposited on a GaAs(110) surface, nanoparticles are formed with gap states, enhancing recombination. Figure 11 shows an STM image and the spectra obtained for a bare GaAs and above a Co nanoparticle. The decay constants obtained for both cases are 223 ns and 42 ns, respectively. As expected, the decay is faster at the Co site.

Furthermore, Fig. 11 shows a topographic image (a) and the map of the decay constant obtained over the surface (b). As shown in the overlap of these two images (c), positional agreement is good. As the cross section shows (d), the decay is fast in the Co regions, which is due to the fact that the gap states enhance recombination.

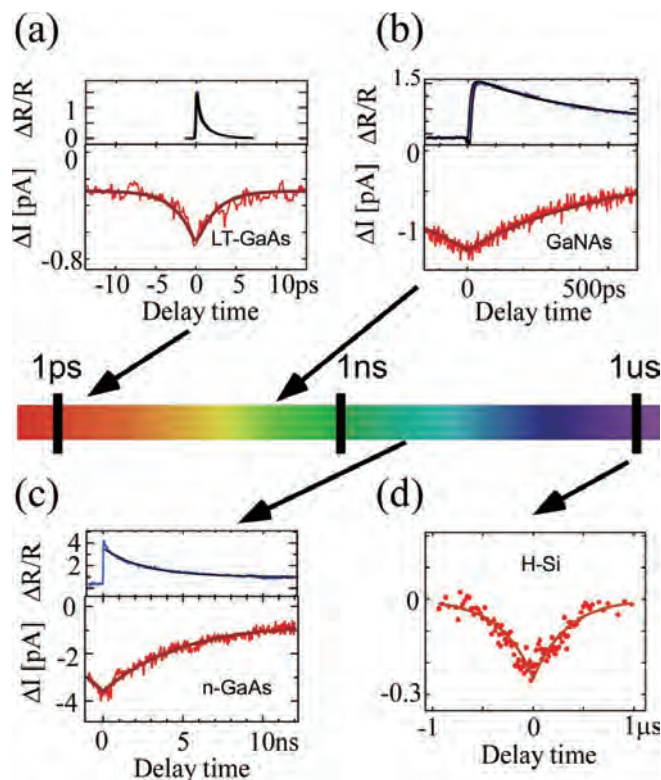


Fig. 10: OPP-STM spectra obtained for various samples. OPP spectra are also shown. (a) LT-GaAs, (b) GaNAs, (c) n-GaAs, and (d) H-terminated Si.

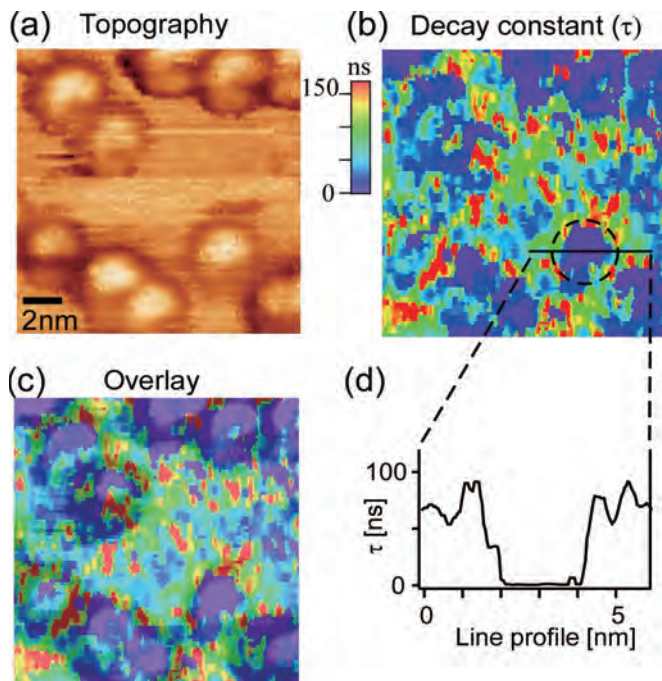


Fig. 11: (a) STM image and (b) decay constant mapping obtained for Co-nanoparticle/GaAs structures. (c) Overlay of (a) and (b). (d) Cross section along line in (b). As shown in (d), a spatial resolution of sub-nm scale is obtained.

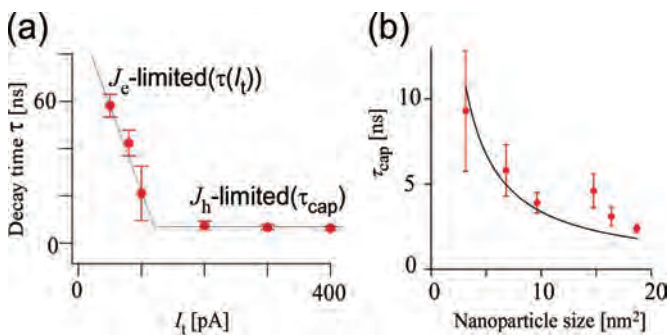


Fig. 12: (a) Decay constant as a function of setpoint current. (b) Hole capture constant (saturated value in (a)) τ_{cap} as a function of Co size.

There are two limitations in this process, i.e., the injection of tunneling current from the STM tip and the capture rate of holes at the gap states. For a sufficient amount of tunneling current, the capture rate becomes the limiting process. Figure 12(a) shows the relationship between the decay constant and the tunneling current. As expected, the decay constant decreased with increasing tunneling current, and had a saturated value of 6.9 ns, which is the hole capture rate of the system, τ_{cap} . The decay process should depend on the gap-state density. Figure 12(b) shows τ_{cap} as a function of nanoparticle size, i.e., density of gap states. As expected, the decay constant increases with decreasing nanoparticle size.

Direct detection of photocurrent

To increase the generality of this microscopy technique and its applicability to various types of material and structure, additional techniques are desired. For example, as an application of TR-STM based on a method similar to the analysis of a molecular electronic structure, a two-photon absorption measurement was used together with TR-STM [47]. In the future, the development of direct techniques for detecting photocurrents in transient dynamics at the nanoscale level is expected to play an important role in determining the optical characteristics of materials and devices.

Here, OPP-STM measurements were carried out on transient photocurrent dynamics in a layered n-type semiconductor, p-WSe₂ [48]. Since WSe₂ has an indirect bulk band gap, the recombination lifetime of photoexcited carriers is significantly long ($\sim 10 \mu\text{s}$) compared with the process of diffusion. Therefore, under a forward bias voltage condition, i.e., negative sample bias voltage, excited electrons are considered to directly tunnel to the STM tip as a photocurrent.

Figure 13 shows the I - V curves measured by LM-STS (see 2.3), where dashed and solid lines indicate the I - V curves obtained without and with laser excitation, respectively. Under an illuminated condition using a CW laser, the negative sample bias-voltage region is divided into two parts: (1) a photovoltaic region and (2) a photoamperic region. Until the conduction band edge reaches the Fermi level (photovoltaic region), the bias voltage is mainly applied to the tunnel gap; therefore, under photoillumination, the SPV, and thereby the tunneling current, strongly depends on the bias voltage. When the negative bias voltage is further increased, the tunneling gap con-

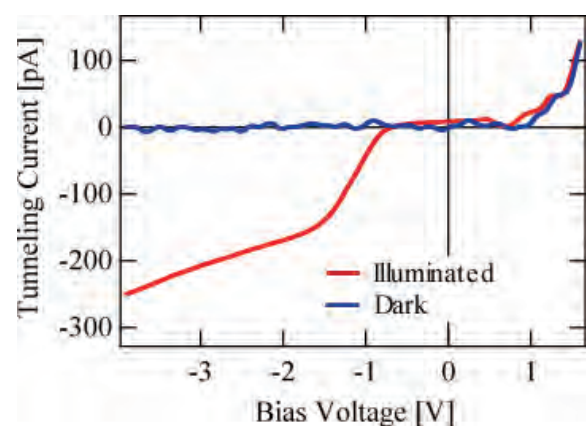


Fig. 13: I - V curves measured under dark (solid line) and illuminated (dashed line) conditions.

ductance becomes higher than that in the space charge region of WSe_2 owing to the reduction in tunneling barrier height for electrons (photoamperic region). Under such a condition, the tunneling current mainly consists of photogenerated carriers from the bulk side. Therefore, the photocurrent depends on the photointensity and the volume of TIBB, where photogenerated carriers drift toward the STM tip. Since the region of TIBB gradually increases as the bias voltage increases, the tunneling current slowly increases with the bias voltage. No current is observed for a negative bias voltage under the dark condition, indicating that the photocurrent is directly detected as a signal via tunneling.

Figure 14 shows a series of time-resolved spectra obtained under various laser intensities. A fast component (decay constant ~ 5 ns) and a slow component (decay constant ~ 200 ns) were observed. For low laser intensities, only the fast component appears and the intensity of the slow component increases with increasing laser intensity.

The photocurrent dynamics reflects the flow of excited photocarriers at the surface, which is determined by the balance between the diffusion and tunneling rates. For low laser intensity, the diffusion rate becomes the limiting factor in the balance, where the tunneling of the excess electrons trapped at the surface during photoexcitation

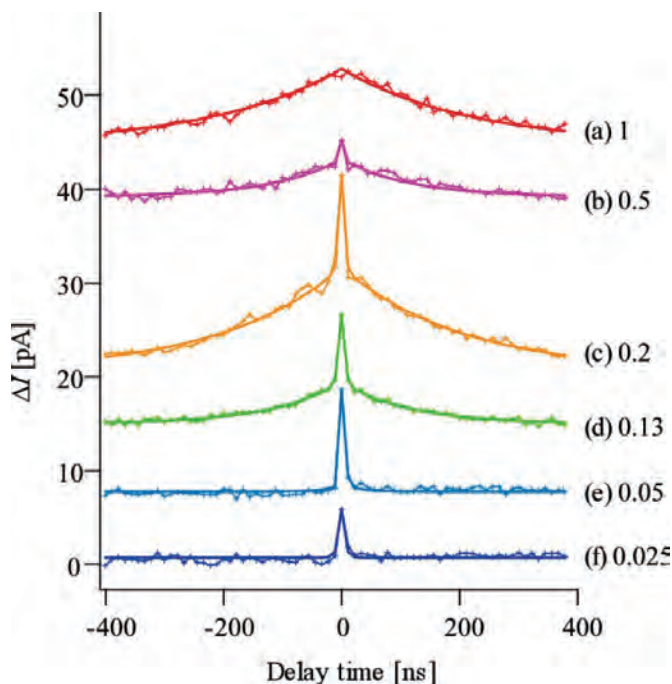


Fig. 14: Series of OPP-STM spectra obtained for different laser intensities. The maximum laser intensity is 0.9 mW and the other values are relative ratios reduced by filters.

is detected dominantly as the signal (fast component, (e), (f), and (g) in Fig. 14). In contrast, for a high laser intensity, the tunneling rate becomes the limiting factor and the diffusion process produces tunneling with a large decay constant (slow component, (a) in Fig. 14). In the intermediate range, the excess electrons trapped at the surface first undergo tunneling. Then, the electrons from the bulk side undergo tunneling at a certain rate of diffusion. As a result, the slow component appears in the time-resolved spectra following the fast component ((b), (c) and (d) in Fig. 14).

To analyze the process for the fast component in more detail, the tunneling current dependence of the fast component was measured. Figure 15(a) shows the series of spectra obtained, and the decay constant τ as a function of the tunneling current is shown in Fig. 15(b). The tunneling current was adjusted by changing the tip-sample distance before each measurement under illumination with the pulse laser. The decay constant τ decreases with increasing tunneling current as expected. The excess minority carriers transiently trapped at the surface for a few nanoseconds, which produce a transient surface photovoltage and cannot be detected by conventional methods, are directly observed by TR-STM

The direct detection of a photoexcited current shown in this section makes this microscopy technique more general and practical.

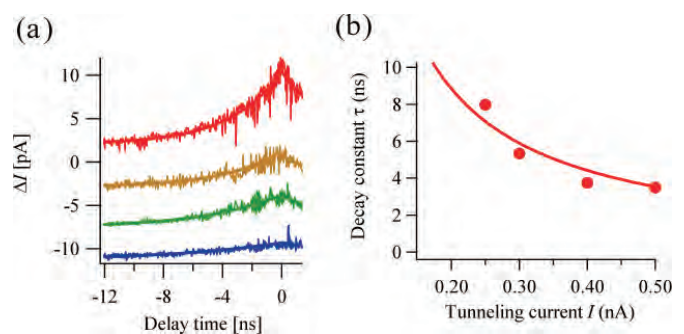


Fig. 15: (a) Series of OPP-STM spectra obtained for different setup tunneling currents. (b) Decay constant as a function of setup tunneling currents.

Future prospects

We have overviewed laser-combined STM and its applications. For further advances, the development of additional techniques is expected. For example, as an application of TR-STM based on a method similar to the analysis of a molecular electronic structure, a two-photon absorption measurement was used together with TR-STM [47]. Direct detection of photoexcited current

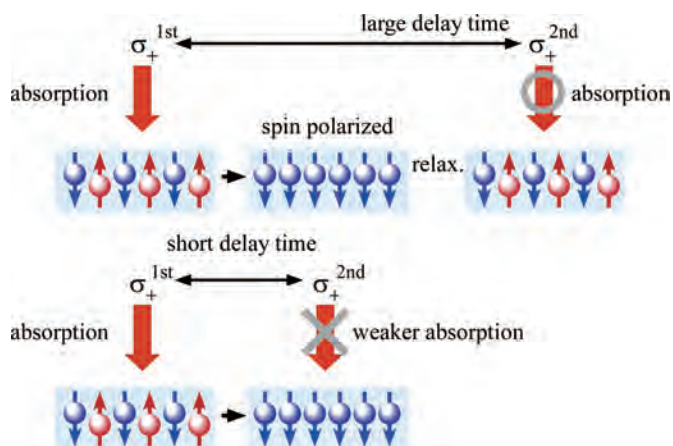


Fig. 16: Schematic illustration for explaining mechanism for measuring spin dynamics, absorption bleaching.

may play an important role. Using circularly polarized light for pump and probe optical pulses, spin dynamics, which has been studied, for example, by spin polarized STM [49, 50], can be observed as has been carried out by the OPP method with optical orientation techniques [51, 52]. The mechanism is similar to that of absorption bleaching. When the down spins excited by the first pulse remain in the excited state, the excitation of the down spins by the second pulse is suppressed depending on the delay time, which is schematically shown in Fig. 16. For example, we have succeeded in observing the relaxation of spins oriented in a single quantum well. By applying an external magnetic field, spin precession was also observed by STM [53].

When the energies of pump and probe pulses are chosen appropriately, excited states may be included in the analysis as in the OPP method. The development of these techniques is considered to increase the generality of this microscopy technique, i.e., when it is more practical and applicable to various phenomena. The essential mechanism of this microscopy technique is the nonlinear interference between the excitations in the transient tunneling current generated by the two laser pulses, therefore, the introduction of new ideas is desired to make further advances. In addition to the use of absorption bleaching mechanism, a new technique is to use terahertz (THz) pulses. Although it is difficult to apply a high bias voltage between the STM tip and sample in general, the tip-enhanced THz monocycle pulses enable it and taking a snapshot of ultrafast dynamics becomes possible [54, 55]. Furthermore, control of the carrier envelope phases (CEP) in pump and probe pulses paves the way for the development of new time-resolved analyses. The physics

and chemistry of nanoscience, such as the molecular dynamics, chemical reactions, phase transitions, and carrier dynamics in functional materials can be explored with sub-cycle time resolution.

SUMMARY

Spectroscopy techniques at the nanoscale level developed by the combination of laser technologies with STM have been overviewed. In the combination of STM with a continuous wave laser, nanoscale analysis of the local potential as well as molecular and atomic structures have been realized. On the other hand, for the combination of STM with ultrashort pulse laser technologies, the spatial resolution of STM and the temporal resolution of an ultrashort pulse laser in the femtosecond range have been simultaneously achieved. With phase-controlled laser pulses, sub-cycle analysis of dynamics can be realized. Following the examples shown in this paper, the development of other new techniques is expected for further advances in this field [54-57].

Acknowledgements: H. S. acknowledges the financial support of a Grant-in-Aid for Scientific Research (17H06088) from the Japan Society for the Promotion of Science.

References

- [1] G. Binning, H. Rohrer, H. Ch. Gerber, E. Weibel, *Phys. Rev. Lett.* 49, 57–61 (1982).
- [2] B. Bhushan, ed., *Scanning Probe Microscopy in Nanoscience and Nanotechnology* (Springer, Berlin, Heidelberg 2010).
- [3] R. Wisendanger, *Scanning Probe Microscopy and Spectroscopy* (Cambridge University Press, Cambridge 1994).
- [4] S. Grafström, *J. Appl. Phys.* 91, 1717-1753 (2002).
- [5] Y. Terada, S. Yoshida, O. Takeuchi, H. Shigekawa *Jnl. Phys. Cond. Mat.* 22, 264008-264015. (2010).
- [6] H. Shigekawa, O. Takeuchi, Y. Terada and S. Yoshida, *Series: Handbook of Nanophysics*, ed. by Klaus Sattler, Taylor & Francis (2010), vol. 6, Principles and Methods.
- [7] M. Ohtsu, ed. *Near-Field Nano/Atom Optics and Spectroscopy* (Springer, Berlin, Heidelberg 1998).
- [8] M. Ohtsu, ed. *Progress in Nano-Electro-Optics II* (Springer-Verlag Berlin Heidelberg 2003).
- [9] M. Ohtsu, ed. *Progress in Nano-Electro-Optics VI* (Springer-Verlag Berlin Heidelberg 2008).
- [10] T. Okuda, T. Eguchi, K. Akiyama, A. Harasawa, T. Kinoshita, Y. Hasegawa, M. Kawamori, Y. Haruyama, S. Matsui, *Phys. Rev. Lett.* 102-105, 105503 (2009).
- [11] A. Saito, J. Maruyama, K. Manabe, K. Kitamoto, K. Takahashi, K. Takami, Y. Tanaka, D. Miwa, M. Yabashi, M. Ishii, Y. Takagi, M. Akai-Kasaya, S. Shin, T. Ishikawa, Y. Kuwahara, M. Aono, *J. Synchrotron Rad.* 13, 220 (2006).
- [12] M. L. Cummings, T. Y. Chien, C. Preissner, V. Madhavan, D. Dising, M. Bode, J. W. Freeland, V. Rose, *Ultramicroscopy* 112, 22-31 (2012).

- [13] I. Schmid, J. Raabe, B. Sarafimov, C. Quitmann, S. Vranjkovic, Y. Pellmont, H.J. Hug, *Ultramicroscopy* 110, 1267-1272 (2010).
- [17] S. Yasuda, T. Nakamura, M. Matsumoto, H. Shigekawa, *J. Am. Chem. Soc.* 125, 16430-16433 (2003).
- [18] A. Troisi, M. A. Ratner, *Small*, 2, 172-181 (2006).
- [19] H. W. Yeom, S. Takeda, E. Rotenberg, I. Matsuda, K. Horikoshi, J. Schaefer, C. M. Lee, S. D. Kevan, T. Ohta, T. Nagao, S. Hasegawa, *Phys. Rev. Lett.* 82, 4898-4901 (1999).
- [20] S. J. Park, H. W. Yeom, S. H. Min, D. H. Park, I. -W. Lyo, *Phys. Rev. Lett.* 93, 106402-106405 (2004).
- [21] S. J. Park, H. W. Yeom, J. R. Ahn, I. -W. Lyo, *Phys. Rev. Lett.* 95, 126102-126105 (2005).
- [22] Y. Terada, S. Yoshida, A. Okubo, K. Kanazawa, M. Xu, O. Takeuchi H. Shigekawa, *Nano Lett.* 8, 3577-3581 (2008).
- [23] R. J. Hamers, K. Markert, *J. Vac. Sci. Technol. A*, 8, 3524-3530 (1990).
- [24] Y. Kuk, R. S. Becker, P. J. Silverman, G. P. Kochanski, *Phys. Rev. Lett.* 65, 456-459 (1990).
- [25] M. McEllistrem, G. Haase, D. Chen, R. J. Hamers, *Phys. Rev. Lett.* 70, 2471-2474 (1993).
- [26] O. Takeuchi, S. Yoshida and H. Shigekawa, *Appl. Phys. Lett.* 84, 3645-3647 (2004).
- [27] S. Yoshida, Y. Kanitani, R. Oshima, Y. Okada, O. Takeuchi, H. Shigekawa, *Phys. Rev. Lett.* 98, 026802-026805 (2007).
- [28] S. Yoshida, Y. Kanitani, O. Takeuchi, H. Shigekawa *Appl. Phys. Lett.* 92, 102105-102107 (2008).
- [29] A. Othonos, *J. Appl. Phys.* 83, 1789-1830 (1998).
- [30] J. Shah, *Ultrafast Spectroscopy of Semiconductors and Semiconductor Nanostructures* (Springer, Berlin, Heidelberg 1999).
- [31] J. Kanasaki, T. Ishida, K. Ishikawa, K. Tanimura, *Phys. Rev. Lett.* 80, 4080-4083 (1998).
- [32] D.N. Futaba, R. Morita, M. Yamashita, S. Tomiyama, H. Shigekawa, *Appl. Phys. Lett.* 83, 2333-2335 (2003).
- [33] J. Kim, M.-L. Yeh, F. S. Khan, J. W. Williams, *Phys. Rev. B* 52, 14709-14718 (1995).
- [34] Y. Sainoo, Y. Kim, T. Okawa, T. Komeda, H. Shigekawa, M. Kawai, *Phys. Rev. Lett.* 95, 246102-246105 (2005).
- [35] B. C. Stipe, M. A. Rezaei, W. Ho, *Science* 280, 1732-1735 (1998).
- [36] K. Makino, J. Tominaga, M. Hase, *Opt. Express*. 19, 1260-1270 (2011).
- [37] H. J. Mamin, H. Birk, P. Wimmer, D. Rugar, *J. Appl. Phys.* 75, 161-168 (1994).
- [38] J. Wintterlin, J. Trost, S. Renisch, R. Schuster, T. Zambelli, G. Ertl, *Surf. Sci.* 394, 159-169 (1997).
- [39] U. Kemiktarak, T. Ndukum, K.C. Schwab, K. L. Ekinci, *Nature* 450, 85-88 (2007).
- [40] G. Nunes Jr, M. R. Freeman, *Science* 262, 1029-1032 (1993).
- [41] N. N. Khusnatdinov, T. J. Nagle, and G. Nunes, *Appl. Phys. Lett.* 69, 2294-2296 (1996).
- [42] R. H. M. Groeneveld and H. van Kempen, *Appl. Phys. Lett.* 77, 4434-4436 (2000).
- [43] G. M. Steeves, A. Y. Elezzabi, and M. R. Freeman, *Appl. Phys. Lett.* 72, 504-506 (1998).
- [44] R. J. Hamers, David G. Cahill, *Appl. Phys. Lett.* 57, 2031-2033 (1990).
- [45] O. Takeuchi, M. Aoyama, R. Oshima, Y. Okada, H. Oigawa, N. Sano, H. Shigekawa, R. Morita, M. Yamashita, *Appl. Phys. Lett.* 85, 3268-3270 (2004).
- [46] Y. Terada, S. Yoshida, O. Takeuchi, H. Shigekawa, *Nature Photonics*, 4, 869-874 (2010).
- [47] S. W. Wu and W. Ho, *Phys. Rev. B* 82, 085444-085451 (2010).
- [48] S. Yoshida, Y. Terada, M. Yokota, O. Takeuchi, Y. Mera, H. Shigekawa, *App. Phys. Exp.* 6, 016601-016604 (2013).
- [49] S. Loth, M. Etzkorn, C. P. Lutz, D. M. Eigler, and A. J. Heinrich, *Science* 329, 1628-1630 (2010).
- [50] J. Brede, B. Chilian, A. A. Khajetoorians, J. Wiebe, R. Wiesendanger, in *Handbook of Spintronics*, ed. By D. Awschalom, J. Nitta, Y. Xu, (Canopus Academic Publishing and Springer, Berlin, Heidelberg, 2012).
- [51] A. Takeuchi, S. Muto, T. Inata, T. Fujii, *Appl. Phys. Lett.* 56, 2213-2215 (1990).
- [52] D. N. Mirlin, in *Optical Orientation*, ed. by F. Meier, B. P. Zakharchenya (North-Holland, Amsterdam, 1984).
- [53] S. Yoshida, Y. Aizawa, Z. Wang, R. Oshima, Y. Mera, E. Matsuyama, H. Oigawa, O. Takeuchi, and H. Shigekawa, *Nature Nanotech*, 9, 588-593 (2014).
- [54] K. Yoshioka, I. Katayama, Y. Minami, M. Kitajima, S. Yoshida, H. Shigekawa, J. Takeda, *Nature Photonics*, 10, 762-765 (2016).
- [55] T. Cocker, D. Peller, P. Yu, J. Repp, and R. Huber, *Nature* 539, 263-267 (2016).
- [56] S. Loth, J. A. J. Burgess, and S. Yan, *Nature nanotech*, 9, 574-575 (2014)
- [57] H. Shigekawa, S. Yoshida, and O. Takeuchi, *Nature Photonics*, 8, 815-817 (2014).



Hidemi Shigekawa is the group leader of the Tsukuba Research Unit for Extreme Quantum Metrology & Quantum Bioscience. He received a doctorate from the University of Tokyo. He was a visiting researcher at Bell Laboratories and worked at the synchrotron radiation facility at Brookhaven National Laboratory. His current research interests are nanoscale science and technologies and he is now leading specially promoted research, supported by Grants-in-Aid for Scientific Research from JSPS (Japan Society for the Promotion of Science) for "Development of sub-cycle time-resolved STM (scanning tunneling microscopy) and its applications".



Shoji Yoshida is an associate professor of University of Tsukuba. He received a doctorate from University of Tsukuba in 2006. His current research target is to develop new microscopy techniques based on scanning tunneling microscopy and ultrashort pulse technologies. He received the Article Award of the Applied Physics Society, Japan in 2015, and is now promoting a Young Scientific Research Fund from JSPS (Japan Society for the Promotion of Science) for "Development of THz-STM".